京都大学学術情報リポジトリ
KURENAI
Kyoto University Research Information Repository

Nonlinear Model Order Reduction of Induction Motors Using Parameterized Cauer Ladder Network Method

Miwa Tobita[1], and Tetsuji Matsuo[1]

[1] Graduate School of Engineering, Kyoto University, Kyoto 6158510, Japan

In this study, we established the nonlinear model order reduction (MOR) of induction motors by parameterizing a multi-port Cauer ladder network (CLN). Appropriate parameters were selected to incorporate nonlinear magnetic characteristics. The parameterized multi-port CLN was applied to the transient analysis of a rotating induction motor. The proposed method reproduced the finite-element analysis results with various driving frequencies and slips. The parameterized multi-port CLN can effectively reduce the computation time for analyses requiring a large number of time steps.

Index Terms—Cauer ladder network, eddy currents, induction motors, magnetic saturation, multi-port model order reduction.

I. INTRODUCTION

THE recent developments in semiconductor technologies have enabled inverters to utilize switching frequencies up to several hundred kilohertz. A major challenge in the eddy-current field simulation of motors with such high frequencies is excessively long computation time, particularly for the transient calculations in control applications.

Model-order reduction (MOR) methods can reduce the computation time of motor analyses [1]-[3]. The Cauer ladder network (CLN) method, which is an efficient MOR method, was extended to a multi-port model [4] and applied to a linear induction motor [5]. However, incorporating magnetic saturation in the MOR methods remains an open problem. For practical applications of induction motor analyses, the nonlinear characteristics of magnetic saturation should be considered when using the MOR method.

This study aims at establishing a nonlinear MOR for induction motors by introducing the concept of parameterization to multi-port CLNs. A parameterized MOR was used to formulate the nonlinear CLN method [6]. The parameterized single-port CLN contains circuit elements represented by functions of the input current. In the parameterized multi-port CLN, the nonlinear magnetic characteristics of iron are incorporated by employing multiple parameters. Because the number of ports is large, the choice of parameters is not straightforward. An appropriate parameter set must be selected to achieve fast analyses that accurately reflect magnetic saturation. To the best of our knowledge, this is the first attempt to apply a nonlinear MOR method to a rotating induction machine with variable motor speed and driving frequency.

II. NONLINEAR CLN FOR INDUCTION MOTORS

A. Basic Equations

The eddy-current field in the FE space is represented by

$$\boldsymbol{K}\boldsymbol{a} = \boldsymbol{\sigma}\boldsymbol{e}, \quad \boldsymbol{C}\boldsymbol{e} = -\frac{\mathrm{d}}{\mathrm{d}t}\boldsymbol{C}\boldsymbol{a}, \tag{1}$$

Corresponding author: M. Tobita (email: tobita.miwa.73x@st.kyoto-u.ac.jp).

where $\boldsymbol{a}$ and $\boldsymbol{e}$ are the variable vectors of the magnetic vector potential and electric field, respectively. $\boldsymbol{\nu}$ and $\boldsymbol{\sigma}$ are the reluctivity and conductivity matrices, respectively, in the analysis domain. Stiffness matrix $\boldsymbol{K}$ is represented by $\boldsymbol{K} = \boldsymbol{C}^{\mathrm{T}}\boldsymbol{\nu}\boldsymbol{C}$, where $\boldsymbol{C}$ is edge-face incident matrix.

Using the procedures described below, the CLN method reduces the electromagnetic field distribution in the finite element (FE) space to the resistance and inductance matrices representing electric and magnetic spatial modes, respectively.

Let the number of ports be M. It is assumed that the electromagnetic field can be expressed by a space mode summation

$$\boldsymbol{a} = \sum_n \boldsymbol{a}_{2n+1}\boldsymbol{I}_{2n+1}, \quad \boldsymbol{e} = \sum_n \boldsymbol{e}_{2n}\boldsymbol{V}_{2n}, \tag{2}$$

where $\boldsymbol{I}_{2n+1}, \boldsymbol{V}_{2n} \in \mathbb{R}^M$ are the current and voltage vectors, respectively, determined by the ladder network [5]. The matrices $\boldsymbol{a}_{2n+1}$ and $\boldsymbol{e}_{2n}$ consist of the basis vectors of the magnetic vector potential and electric field, respectively. Their columnwise expressions are

$$\boldsymbol{a}_{2n+1} = [\boldsymbol{a}_{1,2n+1}, \cdots, \boldsymbol{a}_{M,2n+1}], \tag{3}$$
$$\boldsymbol{e}_{2n} = [\boldsymbol{e}_{1,2n}, \cdots, \boldsymbol{e}_{M,2n}], \tag{4}$$

where $\boldsymbol{a}_{m,2n+1}$ and $\boldsymbol{e}_{m,2n}$ are the nth basis vectors when a unit input is supplied to port m, with no input applied to the other ports.

If the reluctivity, ν, is fixed, the basis matrices have the recurrence relation

$$\boldsymbol{K}(\boldsymbol{a}_{2n+1} - \boldsymbol{a}_{2n-1}) = \boldsymbol{\sigma}\boldsymbol{e}_{2n}\boldsymbol{R}_{2n}, \tag{5}$$
$$\boldsymbol{e}_{2n+2} - \boldsymbol{e}_{2n} = -\boldsymbol{a}_{2n+1}\boldsymbol{L}_{2n+1}^{-1}, \tag{6}$$

where the resistance and inductance matrices are obtained by

$$\boldsymbol{R}_{2n}^{-1} = \boldsymbol{e}_{2n}^{\mathrm{T}}\boldsymbol{\sigma}\boldsymbol{e}_{2n}, \quad \boldsymbol{L}_{2n+1} = \boldsymbol{a}_{2n+1}^{\mathrm{T}}\boldsymbol{K}\boldsymbol{a}_{2n+1}, \tag{7}$$

respectively. The basis matrices satisfy orthogonal relations

$$\boldsymbol{e}_{2i}^{\mathrm{T}}\boldsymbol{\sigma}\boldsymbol{e}_{2j} = \delta_{ij}\boldsymbol{R}_{2i}^{-1}, \quad \boldsymbol{a}_{2i+1}^{\mathrm{T}}\boldsymbol{K}\boldsymbol{a}_{2j+1} = \delta_{ij}\boldsymbol{L}_{2i+1}. \tag{8}$$
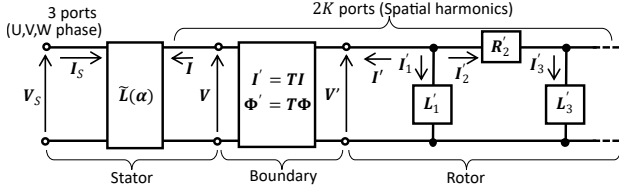
Fig. 1. Parameterized multi-port CLN applied to induction motors. It consists of a stator, interface, and rotor. The stator is parameterized by vector $\boldsymbol{\alpha}$.

B. Construction of Nonlinear Multi-port CLN

For application to an induction motor, the multi-port CLN of the stator and rotor domains are constructed separately and connected by the electromagnetic field on their interface, as shown in Fig. 1. The circuit construction does not require frequency or slip information. In this study, for simplicity, only the stator CLN was parameterized, although rotor parameterization can be achieved by a similar process.

Vectors $\boldsymbol{I}_\mathrm{s}$ and $\boldsymbol{\Phi}_\mathrm{s}$ are source current and magnetic flux with three-phase components represented by $\boldsymbol{I}_\mathrm{s} = [I_\mathrm{U}, I_\mathrm{V}, I_\mathrm{W}]^\mathrm{T}$ and $\boldsymbol{\Phi}_\mathrm{s} = [\Phi_\mathrm{U}, \Phi_\mathrm{V}, \Phi_\mathrm{W}]^\mathrm{T}$, respectively. The source voltage $\boldsymbol{V}_\mathrm{s} = [V_\mathrm{U}, V_\mathrm{V}, V_\mathrm{W}]^\mathrm{T}$ can be derived by $\boldsymbol{V}_\mathrm{s} = \mathrm{d}\boldsymbol{\Phi}_\mathrm{s}/\mathrm{d}t$. Vectors $\boldsymbol{I}$ and $\boldsymbol{\Phi}$ are defined by the spatial harmonics of the circumferential magnetic field H_ϕ and the axial vector potential A_z at the stator side of the interface, where the tangential field H_ϕ at the interface is given as the Neumann boundary condition in the FE formulation. We assume that H_ϕ can be expanded into cosine and sine terms [5] as

$$H_\phi(\phi, t) = \sqrt{2} \sum_{m=\mathrm{odd}} [H_{cm}(t)\cos(mp\phi) \\ + H_{sm}(t)\sin(mp\phi)], \quad (9)$$

where p is the number of pole pairs. The coefficients comprise the vector $\boldsymbol{I}$ as

$$\boldsymbol{I} = [H_{c1}, H_{s1}, \cdots, H_{c2K-1}, H_{s2K-1}]^\mathrm{T}. \quad (10)$$

The subscripts $c2k-1$ and $s2k-1$ denote the cosine and sine components of the $2k-1$ th harmonics, respectively. The harmonic components are defined in the spatial period π/p, and those higher than the $2K-1$ th are truncated. By expanding A_z in the same manner, we define $\boldsymbol{\Phi}$ as

$$\boldsymbol{\Phi} = \frac{\pi r_\mathrm{c}}{p}[A_{c1}, A_{s1}, \cdots, A_{c2K-1}, A_{s2K-1}]^\mathrm{T}, \quad (11)$$

where r_c is the radius of the gap interface. Vectors $\boldsymbol{I}'$ and $\boldsymbol{\Phi}'$ are counterparts on the rotor side, represented by

$$\boldsymbol{I}' = [H'_{c1}, H'_{s1}, \cdots, H'_{c2K-1}, H'_{s2K-1}]^\mathrm{T}, \quad (12)$$

$$\boldsymbol{\Phi}' = \frac{\pi r_\mathrm{c}}{p}[A'_{c1}, A'_{s1}, \cdots, A'_{c2K-1}, A'_{s2K-1}]^\mathrm{T}, \quad (13)$$

respectively. Boundary conditions $H'_\phi = H_\phi$ and $A'_z = A_z$ give the relations

$$\boldsymbol{I}' = \boldsymbol{T}\boldsymbol{I}, \quad \boldsymbol{\Phi}' = \boldsymbol{T}\boldsymbol{\Phi}, \quad (14)$$

where $\boldsymbol{T} = \mathrm{blockdiag}(\boldsymbol{T}_1, \boldsymbol{T}_3, \cdots, \boldsymbol{T}_{2K-1})$ is a rotation matrix with

$$\boldsymbol{T}_m = \begin{bmatrix} \cos(mp\int \omega_\mathrm{R}\mathrm{d}t) & \sin(mp\int \omega_\mathrm{R}\mathrm{d}t) \\ -\sin(mp\int \omega_\mathrm{R}\mathrm{d}t) & \cos(mp\int \omega_\mathrm{R}\mathrm{d}t) \end{bmatrix}, \quad (15)$$

for $m = 1, 3, ..., 2K - 1$. The relationship between the mechanical angular frequency ω_R and synchronous angular frequency ω_s is $\omega_\mathrm{R} = (1 - s)\omega_\mathrm{s}/p$, where s is the slip. The electromotive force in the rotor, generated by the slip, can be incorporated into the CLN using $\boldsymbol{T}$.

In this study, for simplicity, the stator-winding resistance was not included in the CLN, and the iron-core conductivity was neglected. Accordingly, the stator-side CLN is represented by a single stage with a single inductance matrix. The stator equation is

$$\tilde{\boldsymbol{\Phi}} = \begin{bmatrix} \boldsymbol{L}_{00}(\boldsymbol{\alpha}) & \boldsymbol{L}_{10}^\mathrm{T}(\boldsymbol{\alpha}) \\ \boldsymbol{L}_{10}(\boldsymbol{\alpha}) & \boldsymbol{L}_{11}(\boldsymbol{\alpha}) \end{bmatrix} \tilde{\boldsymbol{I}} = \tilde{\boldsymbol{L}}(\boldsymbol{\alpha})\tilde{\boldsymbol{I}}, \quad (16)$$

where $\tilde{\boldsymbol{\Phi}} = [\boldsymbol{\Phi}_\mathrm{s}, \boldsymbol{\Phi}]^\mathrm{T}$ and $\tilde{\boldsymbol{I}} = [\boldsymbol{I}_\mathrm{s}, \boldsymbol{I}]^\mathrm{T}$. The inductance matrix $\tilde{\boldsymbol{L}}$ is treated as a function of the parameter vector $\boldsymbol{\alpha}$ to incorporate the nonlinear magnetic characteristics of the iron core. Various parameters can be chosen for the components of $\boldsymbol{\alpha}$, as described in the next section.

The state equations of the rotor [5] are derived as follows:

$$\boldsymbol{L}'_{2n-1}\frac{\mathrm{d}\boldsymbol{I}'_{2n-1}}{\mathrm{d}t'} - \boldsymbol{L}'_{2n+1}\frac{\mathrm{d}\boldsymbol{I}'_{2n+1}}{\mathrm{d}t'} = \boldsymbol{R}'_{2n}\boldsymbol{I}'_{2n}, \\ \boldsymbol{I}'_{2n} = -\boldsymbol{I}' - \boldsymbol{I}'_1 - \cdots - \boldsymbol{I}'_{2n-1}. \quad (17)$$

The magnetic flux at the interface $\boldsymbol{\Phi}'$ is determined by the first stage of the rotor CLN as $\boldsymbol{\Phi}' = \boldsymbol{L}'_1\boldsymbol{I}'_1$. The substitution of (16) into the boundary condition (14) results in

$$\boldsymbol{\Phi} = \boldsymbol{T}^{-1}\boldsymbol{L}'_1\boldsymbol{I}'_1 = \boldsymbol{L}_{10}\boldsymbol{I}_\mathrm{s} + \boldsymbol{L}_{11}\boldsymbol{I}. \quad (18)$$

The variables $\boldsymbol{\Phi}_\mathrm{s}$, $\boldsymbol{I}$, and $\boldsymbol{\Phi}$ at time t can be derived by solving (16) and (17) with the boundary condition (18) and a given source current $\boldsymbol{I}_\mathrm{s}$. The total input power P_1, air-gap power P_2, and output torque τ are calculated as follows [5]:

$$P_1 = \boldsymbol{V}_\mathrm{s}^\mathrm{T}\boldsymbol{I}_\mathrm{s}, \quad P_2 = -\boldsymbol{V}^\mathrm{T}\boldsymbol{I}, \quad \tau = r_\mathrm{c}\boldsymbol{I}^\mathrm{T}\boldsymbol{B}, \quad (19)$$

where $\boldsymbol{V} = \mathrm{d}\boldsymbol{\Phi}/\mathrm{d}t$, and $\boldsymbol{B}$ is defined by the radial magnetic flux density $B_r = (1/r_\mathrm{c})\partial A_z/\partial\phi$ as

$$\boldsymbol{B} = \pi[A_{s1}, -A_{c1}, \cdots, \\ (2K-1)A_{s2K-1}, -(2K-1)A_{c2K-1}]^\mathrm{T}. \quad (20)$$

III. COMPUTATION RESULTS

The induction motor depicted in Fig. 2(a) was analyzed in the FE space. The stator has 12 slots and 2 pole pairs. The rotor consists of an iron core and 16 rotor bars. The mesh generated in the FE field is shown in Fig. 2(b). The reluctance of stator iron is given by $\nu(\boldsymbol{B}) = \nu_\mathrm{i}[h_1(|\boldsymbol{B}|/B_0)^a + h_2]$, where $\nu_\mathrm{i} = (1/4\pi) \times 10^3$ m/H, $a = 6$, $h_1 = 2$, $h_2 = 1$, and $B_0 = 1$ T. The B-H curve is shown in Fig. 3(a). The iron in the rotor is assumed to have a linear property with reluctivity $(1/4\pi) \times 10^4$ m/H. The conductivity of the rotor bar is 4.0×10^7 S/m.

A Self-archived copy in
Kyoto University Research Information Repository
https://repository.kulib.kyoto-u.ac.jp

京都大学学術情報リポジトリ
KURENAI 紅
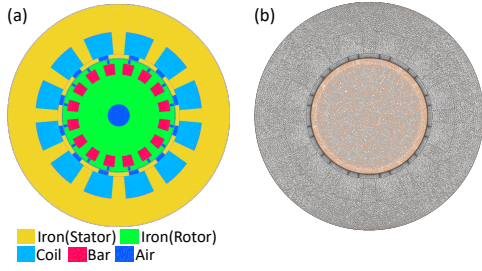Kyoto University Research Information Repository

3

Fig. 2. (a) Induction motor model, (b) mesh generated in the finite element space. The mesh for the stator and rotor domains is shown in different colors.
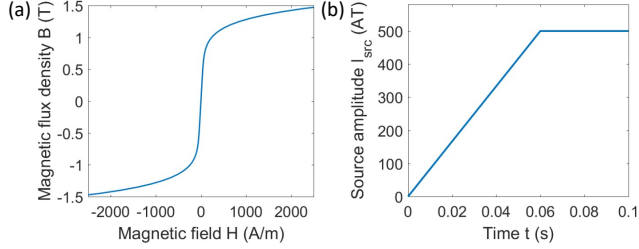

Fig. 3. (a) B-H relation of the iron core in the stator, (b) the amplitude of the input current I_{src}.
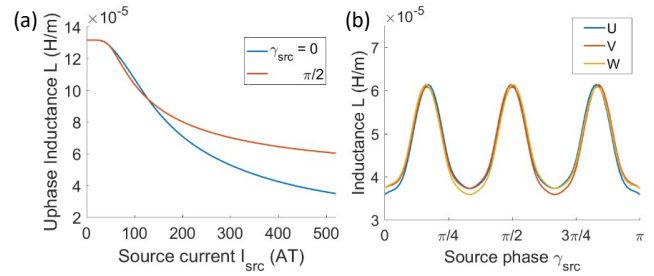

Fig. 4. (a) The U-phase diagonal component, and (b) three-phase diagonal components ($I_{\mathrm{src}} = 500$ AT) of the inductance $\boldsymbol{L}_{00}$.
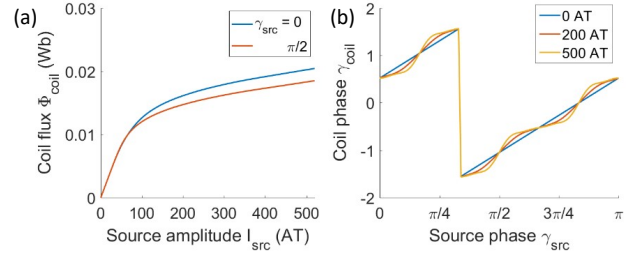

Fig. 5. (a) The coil flux Φ_{coil}, and (b) the coil phase γ_{coil}.

A. Selection of Parameters

In the CLN analysis, a lookup table of the stator inductance matrix was prepared beforehand (offline calculation), and then the state equations were solved (online calculation).

We assumed a balanced three-phase current source

$$\boldsymbol{I}_{\mathrm{s}} = I_{\mathrm{src}} \left[\cos \gamma_{\mathrm{src}}, \cos\left(\gamma_{\mathrm{src}} - \frac{2}{3}\pi\right), \cos\left(\gamma_{\mathrm{src}} - \frac{4}{3}\pi\right) \right]^{\mathrm{T}} \quad (21)$$

where I_{src} and γ_{src} are the current magnitude and phase angle, respectively. The simplest parameterization can be realized by a parameter vector $\boldsymbol{\alpha}_1 = [I_{\mathrm{src}}, \gamma_{\mathrm{src}}]$. For the offline calculation, the reluctivity matrix $\boldsymbol{\nu}$ of the stator was determined by imposing the current source (21) for various $\boldsymbol{\alpha}_1$ with $\boldsymbol{I} = 0$, and the stator inductance matrix was obtained using the determined $\boldsymbol{\nu}$ and unit inputs of $\boldsymbol{I}_{\mathrm{s}}$ and $\boldsymbol{I}$. During the online calculation, we used the stator inductance extracted from the lookup table at $\boldsymbol{\alpha}_1$ by using the spline interpolation.

However, when the rotor influence is significant ($\boldsymbol{I} \neq \boldsymbol{0}$), the source currents, and therefore $\boldsymbol{\alpha}_1$, do not directly represent the degree of magnetic saturation. The magnetic-field distribution inside the stator is more strongly associated with the magnetic fluxes at the source port or interface than the source currents. Hence, we propose other parameter vectors $\boldsymbol{\alpha}_2 = [\Phi_{\mathrm{coil}}, \gamma_{\mathrm{coil}}]$ and $\boldsymbol{\alpha}_3 = [\Phi_{\mathrm{gap}}, \gamma_{\mathrm{gap}}]$, where $[\Phi_{\mathrm{coil}}, \gamma_{\mathrm{coil}}]$ and $[\Phi_{\mathrm{gap}}, \gamma_{\mathrm{gap}}]$ are the amplitude and phase angle of the coil flux and gap flux, respectively, calculated as follows:

$$\Phi_{\mathrm{coil}} = \sqrt{\frac{2}{3}(\Phi_{\mathrm{U}}^2 + \Phi_{\mathrm{V}}^2 + \Phi_{\mathrm{W}}^2)}, \gamma_{\mathrm{coil}} = \tan^{-1}\left(\frac{\Phi_{\beta}}{\Phi_{\alpha}}\right), \quad (22)$$

$$\Phi_{\mathrm{gap}} = \sqrt{(\Phi_{\mathrm{c1}}^2 + \Phi_{\mathrm{s1}}^2)}, \gamma_{\mathrm{gap}} = \tan^{-1}\left(\frac{\Phi_{\mathrm{s1}}}{\Phi_{\mathrm{c1}}}\right). \quad (23)$$

Here, $[\Phi_{\mathrm{U}}, \Phi_{\mathrm{V}}, \Phi_{\mathrm{W}}]$ are components of $\boldsymbol{\Phi}_{\mathrm{s}}$, and $[\Phi_{\mathrm{c1}}, \Phi_{\mathrm{s1}}]$ are the first two components of $\boldsymbol{\Phi}$. Clarke transformation is used

to obtain Φ_{α} and Φ_{β} from Φ_{U}, Φ_{V}, and Φ_{W}. In the offline calculation, a table containing the relation of $\boldsymbol{\alpha}_2$ and $\boldsymbol{\alpha}_3$ to $\boldsymbol{\alpha}_1$ was created from (16)(22)(23) under the condition that $\boldsymbol{I} = \boldsymbol{0}$. During the online calculation, the stator inductance was determined using the inductance lookup table for $\boldsymbol{\alpha}_2$ or $\boldsymbol{\alpha}_3$, where $\boldsymbol{I}$ was not necessarily zero depending on the rotor condition.

B. Stator Inductance

The lookup table of the stator inductance matrices was prepared for $I_{\mathrm{src}} = 0$–631 AT (20 divisions in log scale) and $\gamma_{\mathrm{src}} = 0$–$\pi$ (24 divisions). Fig. 4 shows the stator inductance matrix $\boldsymbol{L}_{00}$, wherein the U-phase diagonal component with the source phase $\gamma_{\mathrm{src}} = 0$ and $\pi/2$ is shown in (a). The inductance decreased as the amplitude increased owing to the magnetic saturation. The difference in inductances between the two phases also resulted from the nonlinear magnetic characteristics. Fig. 4(b) shows the three-phase diagonal components with $I_{\mathrm{src}} = 500$ AT. The inductance was minimum when the source phase was positioned at the center of the stator slots.

Fig. 5 depicts the relation between the state of the source current $\boldsymbol{\alpha}_1$ and coil flux $\boldsymbol{\alpha}_2$ obtained from (22). The coil flux in Fig. 5(a) is saturated because of the nonlinear magnetic characteristics. The difference between the source and coil flux phases in Fig. 5(b) is attributed to the stator structure. Similar tendencies are observed with the gap flux $\boldsymbol{\alpha}_3$.

C. Transient Analyses

As shown in Fig. 3(b), source-current amplitude I_{src} increased from 0 to 500 AT in the first three cycles and remained constant for the last two cycles. The employed frequency ranged from 10 to 100 Hz, and the slip was varied from 0 to 1. Identical circuit parameters were used for all conditions
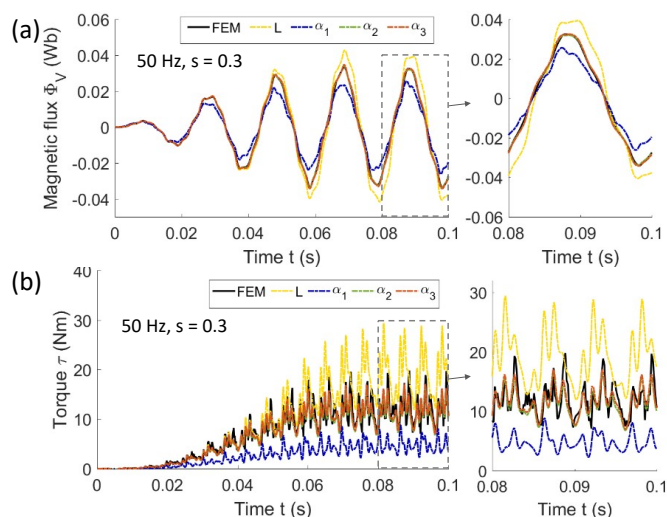
Fig. 6. Transient waveforms of (a) V-phase magnetic flux, and (b) torque. They were obtained using the FEM, linear CLN (L), nonlinear CLN parameterized by the source current ($\boldsymbol{\alpha}_1$), coil flux ($\boldsymbol{\alpha}_2$), and gap flux ($\boldsymbol{\alpha}_3$).
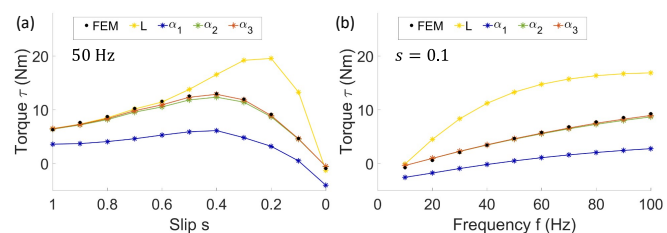

Fig. 7. The torque averaged in the last cycle with various (a) slips, and (b) input frequencies.

because the CLN can incorporate the difference in rotor conditions by modulating the rotation matrix $\boldsymbol{T}$ in (15).

Fig. 6 shows transient waveforms of (a) V-phase magnetic flux Φ_V, and (b) torque τ. The results of the parameterized CLN agree with those of the FE analyses when $\boldsymbol{\alpha}_2$ or $\boldsymbol{\alpha}_3$ are used as the parameters, as predicted in the previous section. Fig. 7 compares the averaged torque in the last cycle with various (a) slips and (b) frequencies. The results indicate that the nonlinear CLN parameterized by $\boldsymbol{\alpha}_2$ or $\boldsymbol{\alpha}_3$ yields results significantly close to those of the FE analysis.

D. Computation Time

The linear solutions dominate the computation time in both FE and CLN analyses. The nonlinear equations were solved by iterating linear solutions using the Newton-Raphson method. The average number of iterations was 5.4 and 7.5 for the FE and CLN calculations, respectively. Hence the transient FE analyses with N_t time-steps required $5.4N_t$ linear solutions.

The CLN method, on the other hand, requires linear solutions only for the offline calculation and not for online calculation. For each stator-CLN parameter, we obtained a single nonlinear solution to determine the reluctivity and 35 linear solutions to determine the inductance matrix (3 phase + 32 harmonic components). The rotor CLN with 2 stages required 32×2 linear solutions to derive $\boldsymbol{R}'$ and $\boldsymbol{L}'$ with 32 harmonic components. Therefore $(7.5 + 35)N_\alpha + 64$ linear

solutions were required for the offline calculation. The online computation time is negligible compared with the offline computation time.

Because the degree of freedom in the full FE analyses is larger than that of the stator or rotor model individually computed in the CLN method, the speedup ratio of the parameterized CLN to transient FE analyses is estimated to be more than $5.4N_t/(42.5N_\alpha + 64)$, which was 4.1 for calculating 20 operating points shown in Fig. 7. The speedup ratio becomes especially large for analyses with a large number of time steps, such as the evaluation of pulse-width modulation (PWM) input with high carrier frequencies, generation of an efficiency map with various frequencies and slips, and coupled analyses with a control circuit.

IV. CONCLUSION

The parameterized multi-port CLN method was developed and applied to an induction motor with nonlinear magnetic characteristics. The developed method reproduced the transient waveforms obtained from FE analysis with various slips and frequencies. The CLN method is more computationally efficient than the FE analyses when the number of time steps is large. Transient analyses with PWM input and the inclusion of iron losses [5] will be considered in further research.

ACKNOWLEDGMENT

REFERENCES

[1] T. Henneron and S. Clenet, "Model order reduction applied to the numerical study of electrical motor based on POD method taking into account rotation movement," *Int. J. Numer. Model. Electron. Network. Dev. Field.,* vol. 27, no. 3, pp. 485-494, 2014.

[2] T. Shimotani, Y. Sato, T. Sato, and H. Igarashi, "Fast finite-element analysis of motors using block model order reduction," *IEEE Trans. Magn.,* vol. 52, no. 3, 7207004, 2015.

[3] L. Montier, T. Henneron, S. Clenet, and B. Goursaud, "Model Order Reduction Applied to a Linear Finite Element Model of a Squirrel Cage Induction Machine Based on POD Approach," *IEEE Trans. Magn.,* vol. 57, no. 6, 3066678, 2021.

[4] T. Matsuo, T. Fujiwara, K. Kuriyama, K. Sugahara, A. Kameari, T. Tokumasu, and Y. Shindo, "Multi-port model order reduction using a matrix cauer ladder network," *IEEE Trans. Magn.,* vol. 56, no. 2, 7506905, 2020.

[5] T. Matsuo, K. Sugahara, A. Kameari, and Y. Shindo, "Model order reduction of an induction motor using a Cauer ladder network," *IEEE Trans. Magn.,* vol. 56, no. 3, 7514704, 2020.

[6] M. Tobita, H. Eskandari, and T. Matsuo, "Model order reduction of nonlinear eddy-current field using parameterized CLN," *COMPEL - Int. J. Comput. Math. Electr. Electron. Eng.,* 2021.